DISPERSIVE SOFT FERRITE MODELS FOR TIME-DOMAIN SIMULATION AND THEIR APPLICATION TO ACCELERATOR COMPONENT MODELING[*]

J.F. DEFORD, G. KAMIN, G.D. CRAIG and L. WALLING[1]

Lawrence Livermore National Laboratory, L-440 Livermore, CA 94550

[1]*Superconducting Super Collider Laboratory, MS 4010 Dallas, TX 75237*

Ferrite has a variety of applications in accelerator components, and the capability to model this magnetic material in the time domain is an important adjunct to currently available accelerator modeling tools. In this paper is described a general dispersive material model which is suitable for a wide variety of media, including ferrite. Based on this model we have developed a representation of the time-domain magnetic properties of PE11BL, the ferrite used in the induction modules of the ETA–II (Experimental Test Accelerator – II) induction linac at LLNL. This material is characteristic of the soft ferrites commonly used in induction accelerators. The model has been implemented in 1–D and 2–D finite-difference time-domain (FDTD) electromagnetic simulators, and comparisons with analytic and experimental results are presented.

KEY WORDS: Electromagnetic field calculations, induction accelerators

1   INTRODUCTION

Soft ferrite found in induction accelerator cells has two principal roles: (1) it acts as an inductive load to the pulse power drive to the cell, and (2) it acts to lower the quality factor (Q) of undesirable rf modes in the cell (see Figure 1). In this paper we will focus on the latter role, in which the material may be characterized by its small signal response. The frequencies of interest are bounded above by the beampipe cutoff of the TE_{1n} (dipole) modes, which for the ETA–II accelerator is $\sim$1.3 GHz. At low frequencies the magnetic response of a polycrystalline NiZn ferrite such as PE11BL (— a photomicrograph of the grain structure of this ferrite is shown in Fig. 2) manufactured by TDK is dominated by the motion of domain walls. At frequencies above $\sim$1 GHz the domain walls can no longer track the applied rf field, and the
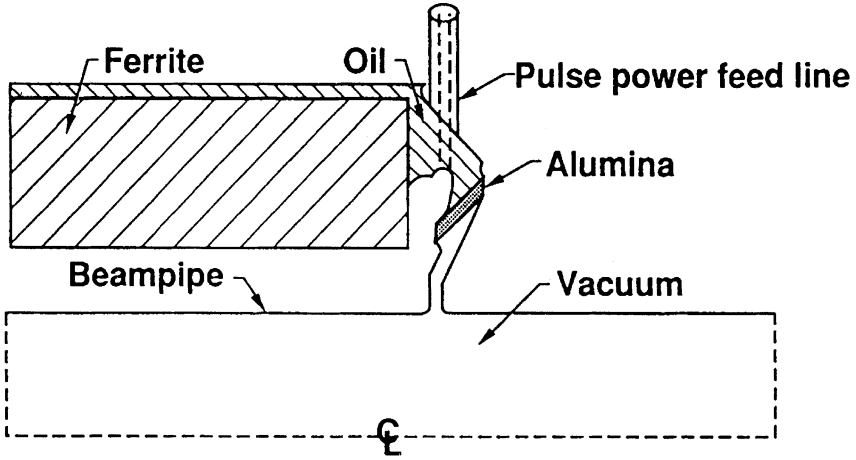
FIGURE 1: Illustration of a cross-section of an ETA-II induction module. Cell is rotationally symmetric about the indicated centerline except for the pulse power feeds (indicated with dashed lines) which enter the cell at two points separated by 180° azimuthally.
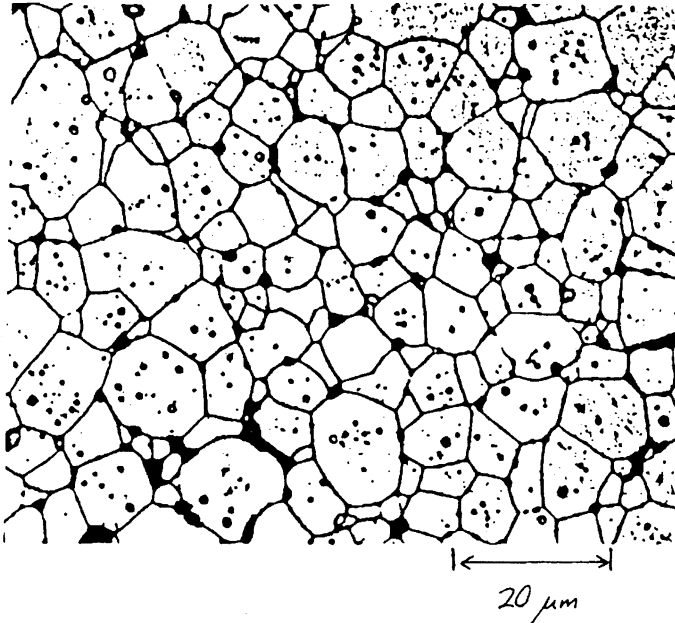

FIGURE 2: Electron micrograph of the grain structure in PE11BL, the ferrite used in the ETA–II accelerator.

response becomes dominated by the ferromagnetic spin resonance of dipoles within the domains.[1]

In general, the small signal response of the material biased with an applied magnetic field is characterized by a tensor permeability with nonzero off-diagonal elements.[2] When there is no preferred direction imposed by an applied magnetic field, or by other means, then the tensor collapses to a scalar. It is this case that we will investigate in this paper. The more general case is a straightforward generalization of this analysis.

Our interest is in calculating the beam coupling impedance associated with an accelerator component such as an induction cavity. The impedance is a very useful quantity in the study of beam-structure interactions and in beam instability analysis in accelerators. The impedance is defined by the relation

$$\vec{Z}(\omega) = \frac{\hat{k}}{c} \tilde{W}_{\parallel} \left(\frac{\omega}{c}\right) - \frac{i}{c} \tilde{\vec{W}}_{\perp} \left(\frac{\omega}{c}\right), \tag{1}$$

where ˜ indicates Fourier transform, c is the velocity of light (and the assumed velocity of the particles), and $\vec{W}$ is the wake potential. The potential is defined as the integral, along the test charge path, of the Lorentz force on the charge due to the source charge as they traverse an accelerator component, i.e.,

$$\vec{W}(s) = \frac{1}{Q} \int_{-\infty}^{\infty} \left[\vec{E} + c\vec{k} \times \vec{B} \right] \Big|_{t=\frac{z+s}{c}} dz. \tag{2}$$

The geometry we assume for the wake potential calculation is illustrated in Figure 3. The interested reader can consult the literature[3-5] for more detailed discussions on the calculation and use of wake potentials and coupling impedances.

Typically, one is interested in broadband information about the impedance spectrum, and time-domain simulation is a natural and powerful technique for generating such a spectrum. In the past the presence of dispersive media such as ferrite has complicated the time-domain simulation problem by requiring a computationally intensive convolution to be performed at every time step. However, Yee,[6] and later Luebbers, et al.,[7] have pointed out that when the frequency dependence of a material constitutive parameter can be represented by simple poles in the complex plane, an algorithm exists for reducing the convolution to a running sum. This discovery greatly simplifies the necessary calculation, and we exploit a variation of Luebbers' method in this work. Bui, et al.,[8] have also recently reported a related technique which they applied to electrically dispersive media in the computation of electromagnetic pulse propagation in human tissue.

2 EXPERIMENTAL CHARACTERIZATION OF PE11BL

In order to determine the frequency dependent permeability for frequencies up to the dipole-mode beampipe cutoff (1.3 GHz), we performed a simple reflection measurement which is illustrated schematically in Figure 4. This measurement was fashioned after an experiment reported by Rado, et al..[1] Some of the material properties of PE11BL are shown in
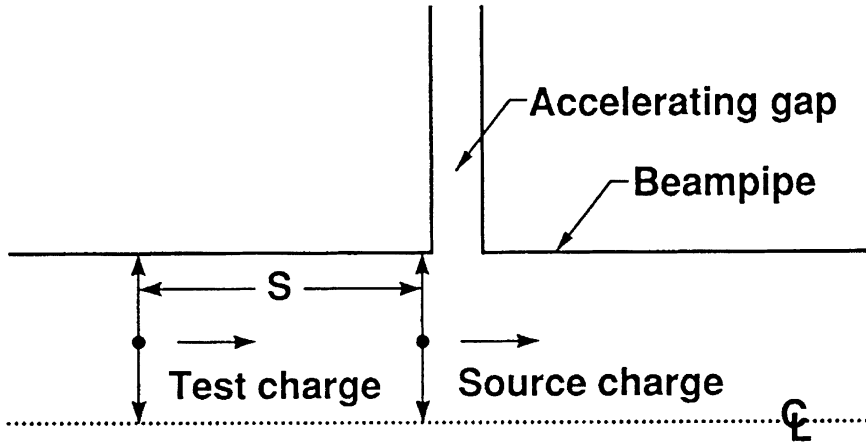
FIGURE 3: Geometry assumed in the definition of the wake potential. Source and test charge move axially ($+z$ direction) through an evacuated beampipe. The charges move with velocity of light in vacuum, a situation which is well approximated in any high energy electron machine. The relative position of the test charge with respect to the source charge is fixed.
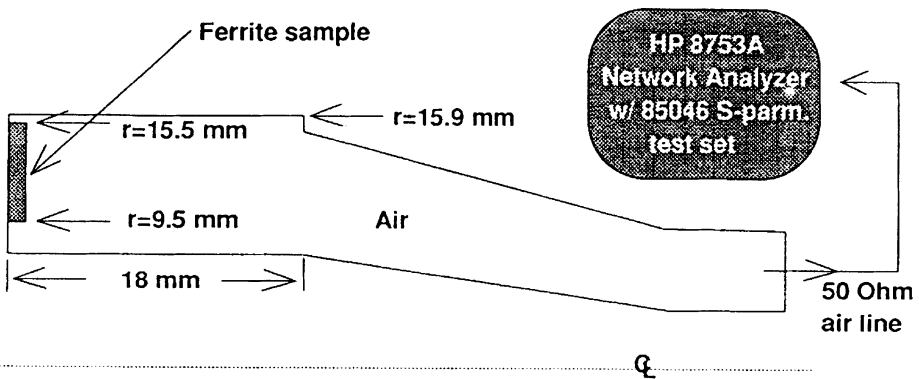

FIGURE 4: Schematic of experimental setup used to measure the permeability of PE11BL ferrite.

TABLE 1:   Properties of PE11BL (from TDK data sheets and direct measurements). T_c = Curie temperature; B_s = saturation magnetization; B_r = remanent magnetization; ρ = bulk resistivity; H_c = coersive force.

	PE11BL (ETA–11 ferrite)
T_c	130°C
B_s	.33 T
B_r	.11 T
ρ	$10^3\,\Omega{\cdot}m$
H_c	20 A/m

Table 1. Small annular samples of the ferrite (I.D. 1.9 cm, O.D. 3.1 cm) were milled to axial thicknesses of 1 mm and 2 mm. To measure the bulk permeability a sample was placed at the shorted end of a $\sim 50\Omega$ coaxial fixture that mated to a network analyzer through a 50Ω air line. The network analyzer was then used to measure the S_{11} scattering matrix coefficient over the desired frequency range. The placement of the toroidal samples against the shorted end of the coaxial line insured that the value of the permittivity of the samples had a negligible effect on the measurement.

Reflection measurements were taken on both 1 mm and 2 mm thick samples, for the purposes of checking the method, and to test for reproducibility in the results. Additionally, several of the samples were measured, then heated above the Curie temperature, allowed to cool, and then remeasured to test for effects of possible residual magnetization. No measurable effects were noted.

The reflection coefficient as a function of material constitutive parameters and wave number is given by the expression for normal incidence reflection from a slab backed by a perfect electric conductor, i.e.,

$$R = \frac{\left[\left(1 + e^{-i2k\Delta}\right) - \eta_r\left(1 - e^{-i2k\Delta}\right)\right]e^{i2k_o\Delta}}{\left(1 + e^{-i2k\Delta}\right) + \eta_r\left(1 - e^{-i2k\Delta}\right)}, \qquad (3)$$

where Δ is the sample thickness, $\eta_r = \sqrt{\frac{\mu_r}{\epsilon_r}}$ is the relative wave impedance of the ferrite, k is the wave number in the ferrite, and k_o is the free-space wave number. R as shown in Equation (3) has been normalized by the reflection obtained when no material is present. When the sample is thin compared to a material wavelength, then the relative permeability, μ_r, is related to R by the equation

$$\mu_r \approx 1 - \frac{1 - R}{2k_o\Delta}. \qquad (4)$$

In practice we use Equation (4) to obtain an initial estimate of μ_r, and then iterate on Equation (3) to get the exact solution. The value of μ_r derived in this manner as a function of frequency is shown in Figure 5. The data presented in Figure 5 has been
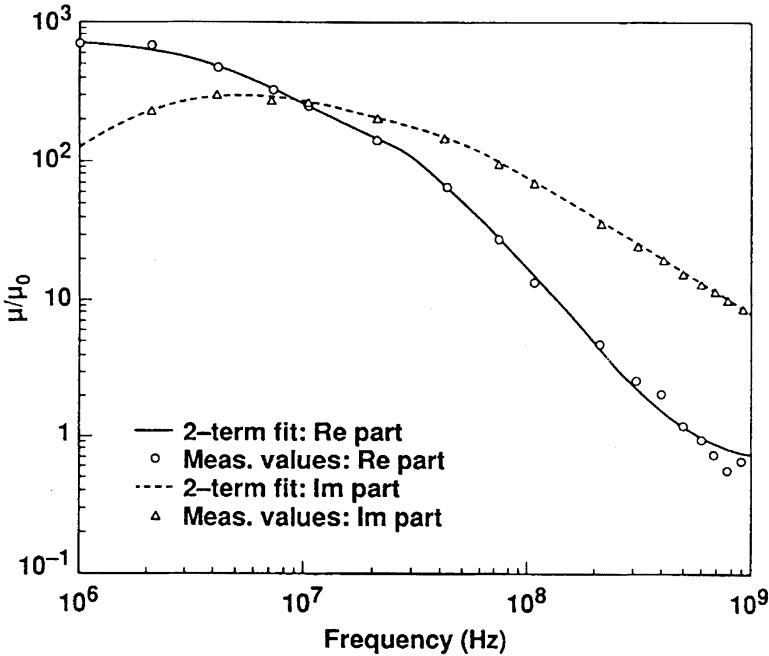
FIGURE 5: Experimental data, and 2-term fit to the experimental data, for the permeability of the PE11BL ferrite. Parameters used in fit are: $\alpha_1 = 6.67 \times 10^{10}$, $\beta_1 - \gamma_1 = 1.77 \times 10^8$, $\beta_1 + \gamma_1 = 1.00 \times 10^{11}$, $\alpha_2 = 2.97 \times 10^{10}$, $\beta_2 - \gamma_2 = 2.73 \times 10^7$, $\beta_2 + \gamma_2 = 1.00 \times 10^{11}$ (See Equation 9). The dielectric constant for PE11BL, $\epsilon_r = 13$, is assumed to be independent of frequency for the purposes of this paper.

corrected by a multiplicative factor (1.3) to account for the difference between short area and sample area.

3   RELAXATION MODEL OF FERRITE PERMEABILITY

Generally, when a broadband response is desired from a frequency-dependent medium, it is necessary to compute a convolution in the time domain. Specifically, when the medium is magnetically dispersive and we can characterize it with a scalar permeability, we have

$$\vec{B}(\omega) = \mu_0 \left(1 + \chi_m(\omega)\right) \vec{H}(\omega) \longrightarrow \vec{B}(t) = \mu_0 \left[\vec{H}(t) + \int_{\tau=0}^{t} \tilde{\chi}_m(t-\tau) \vec{H}(\tau) d\tau \right], \quad (5)$$

where $\tilde{\chi}_m(t)$ is the Fourier transform of the magnetic susceptibility $\chi_m(\omega)$, and we refer to it as the magnetic response function of the material.

As indicated by Luebbers, et al.,[7] when a material has a response function of the form

$$
\tilde{\chi}_m(t) = \begin{cases} \sum_l \alpha_l e^{i\omega_l t}, & t > 0; \\ \\ 0, & t \le 0, \end{cases}
\tag{6}
$$

the convolution in Equation (5) becomes

$$
\vec{B}(t) = \mu_0 \left[\vec{H}(t) + \sum_l \alpha_l e^{i\omega_l t} \vec{f}_l(t) \right],
\tag{7}
$$

where $\vec{f}_l(t) = \int_{\tau=0}^{t} e^{-i\omega_l \tau} \vec{H}(\tau) d\tau$ is a running sum, thus eliminating the necessity to store values of $\vec{H}$ at previous time steps in the simulation. This simple observation, and the fact that the permeabilities of a large class of interesting materials may be accurately represented using sums of exponentials, has important implications for time-domain modeling. Eliminating the need to store previous values of the fields makes it possible to model realistic media in the time-domain with relatively little increase in the computational requirements over non-dispersive media, and one method of exploiting the observation is outlined below.

At frequencies below the ferromagnetic resonance, the following form for $\tilde{\chi}_m(t)$ is appropriate:

$$
\tilde{\chi}_m(t) = \begin{cases} \sum_l \alpha_l e^{-\beta_l t} \sinh(\gamma_l t), & t > 0; \\ \\ 0, & t \le 0, \end{cases}
\tag{8}
$$

which yields a complex magnetic susceptibility of the form

$$
\chi(\omega) = \sum_l \frac{\alpha_l \gamma_l}{(\beta_l + i\omega)^2 - \gamma_l^2},
\tag{9}
$$

where α_l, β_l, and γ_l are all real, and $\beta_l > \gamma_l \ge 0$.

We obtain Equation (8) by arguing first that an instantaneous response of the magnetization in a material to a change in the applied field is unphysical. This requires that $\tilde{\chi}_m(0) = 0$, which in turn demands that the poles come in pairs, and thus we get the sinh term. Secondly, at frequencies significantly below the ferromagnetic resonance, the magnetization physics is dominated by the motion of domain walls that vary widely in their size and shape, and thus their resonant frequencies. The macroscopic response of this type of system may be reasonably approximated with a relaxation model. If there is interest in frequencies at or above resonance, then a term of the form $\alpha e^{-\beta t} \sin(\gamma t)$ must be added to Equation (8) to obtain an accurate representation of the material.

To obtain the adjustable parameters in Equation (9) for a specific material requires a pole extraction from the given susceptibility function. For the purposes of this paper
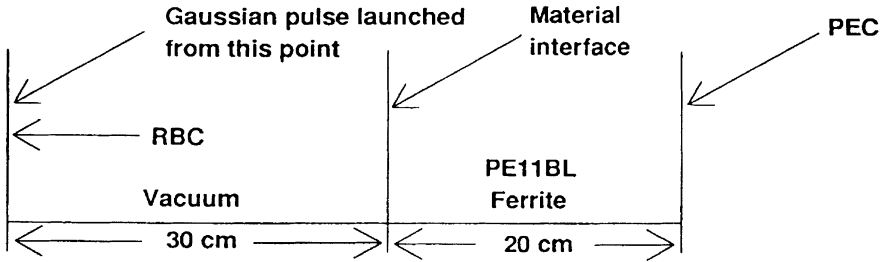
FIGURE 6a: 1–D slab reflection problem geometry. PEC = perfect electric conductor; RBC = radiation boundary condition.
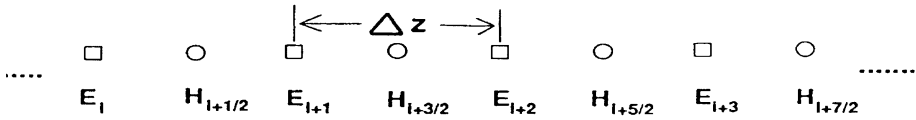

FIGURE 6b: Distribution of field components in 1–D FDTD simulation.

we wrote a simple program that did an exhaustive search in a localized region of parameter space for the optimal values of α, β, and γ to obtain the fit to experimental data shown in Figure 5.

4   1–D MODEL

To study the numerical characteristics of the dispersive media model we conducted a series of tests using the finite-difference time-domain (FDTD) [9] technique in one dimension. The problem geometry and field distribution are shown in Figure 6. The FDTD updating equations and field distribution are obtained by replacing all spatial and temporal derivatives in the Maxwell curl equations with their center-differenced equivalents. This prescription leads to a scheme which is explicit and second order in time and space. When the material is non-dispersive the updating equations in 1–D are easily obtained:

$$\frac{\partial E_x}{\partial z} = -\frac{\partial B_y}{\partial t} = -\mu \frac{\partial H_y}{\partial t} \tag{10}$$

yields

$$H_{j+1/2}^{n+1/2} = H_{j+1/2}^{n-1/2} - \frac{\Delta t}{\mu \Delta z}\left(E_{j+1}^n - E_j^n\right). \tag{11}$$

where the superscripts indicate the time step, and the subscripts indicate the spatial position. Similarly, for the electric field update, we have

$$\frac{\partial H_y}{\partial z} = -\frac{\partial D_x}{\partial t} = -\epsilon \frac{\partial E_x}{\partial t} \tag{12}$$

which yields

$$E_j^{n+1} = E_j^n - \frac{\Delta t}{\epsilon \Delta z}\left(H_{j+1/2}^{n+1/2} - H_{j-1/2}^{n+1/2}\right). \tag{13}$$

When the material is dispersive, the situation is complicated by the convolution which must be done. Any given media exhibits both electric and magnetic dispersion, but for the purposes of this discussion we restrict ourselves to the analysis of magnetic dispersion. The simulation of electric and magnetic dispersion effects simultaneously is the subject of a future paper. To determine the update equation for the magnetic field, we proceed in the following manner:

$$\frac{\partial E_x}{\partial z} = -\frac{\partial B_y}{\partial t} = -\mu_0 \frac{\partial H_y}{\partial t} - \mu_0 \frac{\partial}{\partial t} \int_{\tau=0}^{t} \tilde{\chi}_m(t-\tau) H_y(\tau) d\tau. \tag{14}$$

Assuming the magnetic response function $\tilde{\chi}_m$ is of the form given in Equation (8), we have

$$\frac{\partial E_x}{\partial z} = -\mu_o \frac{\partial H_y}{\partial t} + \frac{\mu_0}{2}\sum_l \alpha_l\left[A_l \int_{\tau=0}^{t} e^{-A_l(t-\tau)} H_y(\tau)d\tau - B_l \int_{\tau=0}^{t} e^{-B_l(t-\tau)} H_y(\tau)d\tau\right], \tag{15}$$

where $A_l = \beta_l - \gamma_l$ and $B_l = \beta_l + \gamma_l$. The discrete form of Equation (15) is given by

$$H_{j+1/2}^{n+1/2} = H_{j+1/2}^{n-1/2} - \frac{\Delta t}{\mu_0 \Delta z}\left(E_{j+1}^n - E_j^n\right) + \frac{(\Delta t)^2}{2}\sum_l \alpha_l A_l \sum_{p=0}^{n-1} e^{-A_l(n-p-1/2)\Delta t} H_{j+1/2}^{p+1/2}$$

$$- \frac{(\Delta t)^2}{2}\sum_l \alpha_l B_l \sum_{p=0}^{n-1} e^{-B_l(n-p-1/2)\Delta t} H_{j+1/2}^{p+1/2}. \tag{16}$$

Defining two auxiliary functions, R and S, which can be updated recursively, using

$$R_{l,j+1/2}^n = \sum_{p=0}^{n-1} e^{-A_l(n-p-1/2)\Delta t} H_{j+1/2}^{p+1/2}, \tag{17}$$

$$S_{l,j+1/2}^n = \sum_{p=0}^{n-1} e^{-B_l(n-p-1/2)\Delta t} H_{j+1/2}^{p+1/2}, \tag{18}$$

yields the following set of update equations for the magnetic field:

$$H_{j+1/2}^{n+1/2} = H_{j+1/2}^{n-1/2} - \frac{\Delta t}{\mu_0 \Delta z} \left(E_{j+1}^n - E_j^n \right)$$

$$+ \frac{(\Delta t)^2}{2} \sum_l \alpha_l \left[A_l R_{l,j+1/2}^n - B_l S_{l,j+1/2}^n \right], \tag{19}$$

$$R_{l,j+1/2}^n = e^{-A_l \Delta t/2} \left[H_{j+1/2}^{n-1/2} + e^{-A_l \Delta t/2} R_{l,j+1/2}^{n-1} \right], \tag{20}$$

$$S_{l,j+1/2}^n = e^{-B_l \Delta t/2} \left[H_{j+1/2}^{n-1/2} + e^{-B_l \Delta t/2} S_{l,j+1/2}^{n-1} \right]. \tag{21}$$

When the electric dispersion is ignored, as in this case, the electric field update is given by Equation (13). The auxiliary functions are real, which leads to the conclusion that the amount of additional storage needed (per field component) to implement this scheme is $2N_p$ real numbers, where N_p is the number of terms in the expansion of the susceptibility (Eq. (9)). The number of floating point operations required (per field component updated using dispersion model) is $10N_p + 4$ in 1–D, up from 3 when the media is nondispersive.

To test the method and its implementation we solved the 1–D reflection problem illustrated in Figure 6a using the parameterization obtained for the PE11BL ferrite. A short Gaussian pulse ($\sigma_t = .5$ ns) was impinged on the ferrite slab, and the normalized reflection coefficient was obtained for the frequency range 0–3 GHz by taking the ratio of the Fourier transforms of the incident and reflected pulses. These data are compared with the analytic result in Figure 7, with excellent agreement.

The magnetic dispersion model has been implemented in the $2\frac{1}{2}$–D FDTD wakefield code AMOS [10], and a 2–D analog to the slab reflection problem was used as a test case. Specifically, we computed the reflection of a pulse from a ferrite load in a shorted coaxial transmission line. Again, excellent agreement with the analytic result was obtained (see Figure 8).
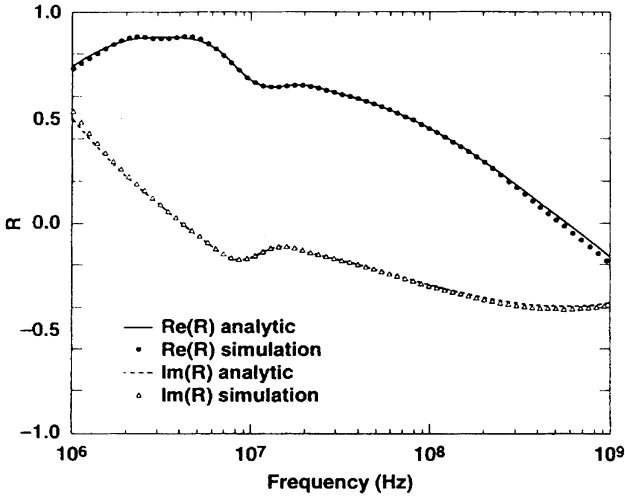
FIGURE 7: Analytic and simulated values of the reflection coefficient for the 1–D problem involving normal incidence on a dispersive ferrite slab (PE11BL) backed by a perfect electric conductor. Spatial cell size in simulation was Δz=.5mm, and reflection reported at surface of slab.
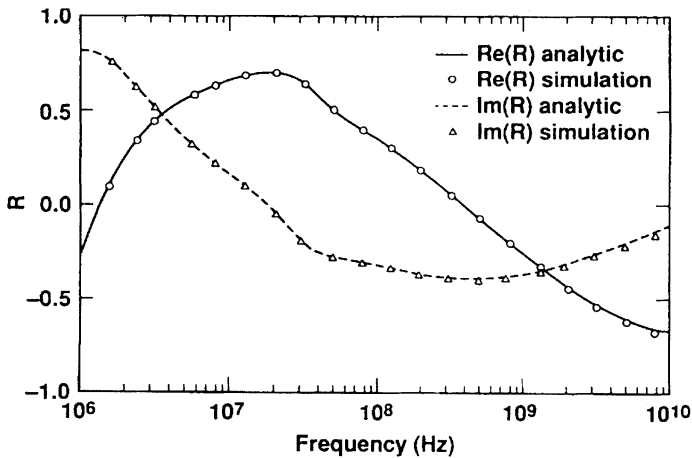

FIGURE 8: AMOS calculation vs. analytic result of the reflection coefficient in a shorted coaxial transmission line loaded with a ferrite toroid. Ferrite used in simulation has same properties as PE11BL listed in Table 1 and caption of Figure 5, except that dielectric constant ϵ_r=20. Axial length of toroid L=5.0cm, inner coax radius $R_i = 6.5$mm, outer coax radius R_o=8.25mm, and grid cell size was Δr=.25mm, Δz=.25mm. Reflection reported at position just in front of toroid in coax.

5   AMOS APPLICATION: ETA–II INDUCTION CELL

The ETA–II [11] induction linac is a high current electron machine, producing a 6 MeV, 3 KA beam for generating high power microwaves. Because of the large beam current, the machine is subject to a possible transverse beam instability known as beam breakup (BBU),[12] and so the transverse dipole coupling impedance of the induction module is of particular interest.

AMOS has been used to study the impedances of the ETA–II induction cell using the dispersive ferrite model described above. A cross-sectional diagram of this cell is shown in Figure 1. The cell is rotationally symmetric about the indicated centerline, with the exception of pulse power feed lines whose center conductors penetrate the outer shell at two locations 180° apart and connect to the base of the ferrite core as shown. When the cables are ignored in the simulation (but left in during the experimental measurement) one gets reasonable agreement between the model and the experiment for the dipole component of the transverse (radial component) coupling impedance (see Figure 9). The technique used to measure the impedance is the "two-wire" method described elsewhere,[13] and the experimental data presented are for two cases: (1) single cell measurement; (2) double cell measurement, with the resulting values halved to get an equivalent single cell impedance. Both measurements were taken with the wires in a plane 90° from the plane of the drive rods, which show the least perturbation resulting from the rods.

The AMOS result shows best agreement with the two-cell measurement. The single-cell measurement exhibits two features that are not present in either the two-cell data or the AMOS result, these being the peak at approximately 700 MHz, and an approximately 100
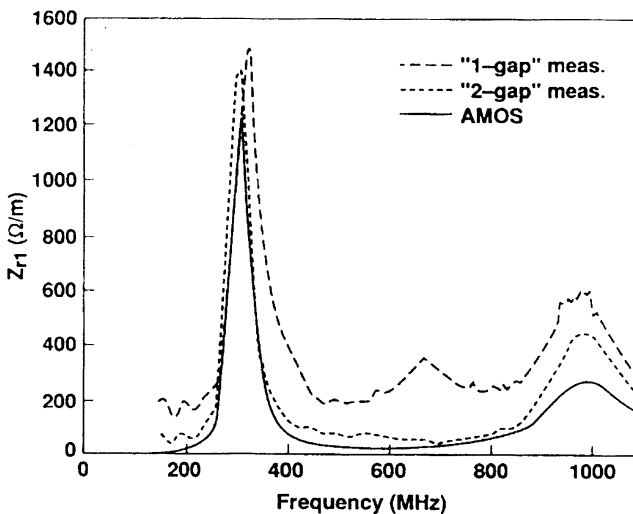

FIGURE 9:   Comparison of experimental data and AMOS calculation for transverse dipole impedance of ETA-II induction module.

Ω/m baseline impedance. The former corresponds in frequency to an $m = 3$ mode, and may show up as a result of the measurement wires being too far apart in the single gap measurement. The two-wire technique will in general yield information about coupling to all modes with odd azimuthal symmetry, although the coupling strength falls off as the wire separation to the power $2m - 1$. For wires sufficiently close together this coupling law will ensure that only the dipole mode contributes significantly to the measured impedance, but increasing the wire separation will eventually lead to measurable contributions from the higher order modes. The 100 Ω/m baseline apparent in the single-cell measured data is not understood at present, and measurements on other cells did not show this baseline. Measurements on simple structures with known coupling impedances suggest that the experimental data are good to $\pm20\%$.

The pulse power feed cables introduce the potential for azimuthal mode coupling and mode splitting. At the relatively low frequencies that we are considering, the degree to which the cables disturb the dipole modes that are important to BBU depends on the relative impedance of the cable and the TEM line formed by the ferrite load. Experimental measurements on similar cavities (DARHT induction modules) with and without the cables show some differences between dipole impedance measured with the two wires in the plane of the feed lines vs. measurements with the wires in the plane perpendicular to the feed lines.

6 CONCLUSIONS

Time-domain simulation of media has long been hampered by inefficient methods for including the dispersive effects of media. The recent realization that materials with exponential response functions could be handled efficiently has revolutionized dispersive media modeling, making it computationally inexpensive for a wide variety of materials.

An implementation of a dispersive media model, and its application in 1 and 2 dimensions, is discussed in this paper. The PE11BL ferrite was characterized over a broad frequency range, and 1–D numerical experiments were performed which showed excellent agreement between simulated and analytic reflection coefficients over several decades in frequency. The models have been implemented in the AMOS wakefield code, and calculations of the transverse coupling impedance of an induction module in the ETA–II accelerator was presented. These data showed good agreement with the impedance values obtained experimentally using the two-wire measurement technique.

A dielectric dispersion model has recently been installed into AMOS in order to accurately characterize the electrical properties of ferrites and other materials, and the combined effects of magnetic and electric dispersion in simulation will be discussed in a forthcoming paper.

REFERENCES

1. G.T. Rado, R.W. Wright, and W.H. Emerson, "Ferromagnetism at very high frequencies. III. Two mechanisms of dispersion in a ferrite," *Physical Review*, **80** (1950) 273–280.

2. R.F. Soohoo, *Theory and Application of Ferrites*, Prentice-Hall, NJ (1960) pp. 60–66.

3.   P. Wilson, "Introduction to wakefields and and wake potentials," **SLAC PUB-4547**, SLAC, Stanford University, Stanford, CA (1989).

4.   T. Weiland, "Comment on wake field computation in time domain," *Nuclear Instruments and Methods*, **216**, (1983) 31–34.

5.   J.F. DeFord and G.D. Craig, "Wake potential and impedance calculations for stiff subrelativistic beams," *Particle Accelerators*, **37–38**, (1992) 111–121.

6.   K. Yee, M. Loyd, and D. Oakley, "The formulation and numerical calculation in the time domain of a two-wire transmission line including frequency-dependent properties," **UCRL-75007**, Lawrence Livermore National Laboratory, Livermore, CA, (1973).

7.   R. Luebbers, et al., "A frequency-dependent finite-differencetime-domain formulation for dispersive materials," *IEEE Transactions on Electromagnetic Compatibility*, **EMC–32**, (1990) 222–227.

8.   M.D. Bui, S.S. Stuchly, and G.I. Costache, "Propagation of transients in dispersive dielectric media," *IEEE Transactions on Microwave Theory and Techniques*, **39**, (1991) 1165–1172.

9.   K.S. Yee, "Numerical solution of initial boundary value problems in isotropic media," *IEEE Transactions on Antennas and Propagation*, **AP–14**, (1966), 302–307.

10.   J.F. DeFord, G.D. Craig, and R.R. McLeod, "The AMOS wakefield code," *Proceedings of the Conference on Computer Codes and the Linear Accelerator Community*, Los Alamos, New Mexico, (1990) pp. 265–289 (also UCRL-102731).

11.   J.C. Clark, et al., "Design and initial operation of the ETA-II induction accelerator," *Proceedings of the 1988 Linear Accelerator Conference*, Williamsburg, VA, (1988), pp. 19–23.

12.   R.J. Briggs, D.L. Birx, G.J. Caporaso, V.K. Neil, and T.C. Genoni, "Theoretical and experimental investigation of the interaction impedances and Q values of the accelerating cells in the Advanced Test Accelerator," *Particle Accelerators*, **18**, (1985) 41–62.

13.   L.S. Walling, D.E. McMurray, D.V. Neuffer, and H.A. Thiessen, "Transmission-line impedance measurements for an advanced hadron facility," *Nuclear Instruments and Methods in Physics Research*, **A281** (1989) 433–447.